Behaviour and design of composite beams subjected to negative bending and compression

Journal of Constructional Steel Research 79 (2012) 34–47

Contents lists available at SciVerse ScienceDirect

Journal of Constructional Steel Research

Behaviour and design of composite beams subjected to negative bending and compression

G. Vasdravellis *, B. Uy, E.L. Tan, B. Kirkland

University of Western Sydney, Sydney, Australia

ARTICLE INFO

Article history:
Received 6 February 2012
Accepted 25 July 2012
Available online 16 August 2012

Keywords:
Composite beams
Negative bending
Compression
Finite element models
Interaction

ABSTRACT

This paper investigates the behaviour of steel–concrete composite beams subjected to the combined effects of negative bending and axial compression. For this study, six full-scale tests were conducted on composite beams subjected to negative moment while compression was applied simultaneously. The level of the applied axial compression varied from low to high. Following the tests, a nonlinear finite element model was developed and calibrated against the experimental results. The model was found to be capable of predicting the nonlinear response and the ultimate failure modes of the tested beams. The developed finite element model was further used to carry out a series of parametric analyses on a range of composite sections commonly used in practice. It was found that, when a compressive load acts in the composite section, the negative moment capacity of a composite beam is significantly reduced and local buckling in the steel beam is more pronounced, compromising the ductility of the section. Rigid plastic analysis based on sectional equilibrium can reasonably predict the combined strength of a composite section and, thus, can be used conservatively in the design practice. Detailing with longitudinal stiffeners in the web of the steel beam in the regions of negative bending eliminate web buckling and increase the rotational capacity of the composite section. Based on the experimental outcomes and the finite element analyses a simplified design model is proposed for use in engineering practice.

1. Introduction

Composite construction of steel and concrete is a popular structural method due to its numerous advantages against conventional solutions. The optimal combination of the properties of the two most popular construction materials, i.e. steel and concrete, results in structures that are both safe and economic. Composite action between the steel beam and the reinforced concrete slab, which is commonly achieved through the welding of shear studs to the top flange of the beam, results in significant reduction of beam deflections, enabling the use of smaller steel sections compared with bare steel systems.

Continuous composite beams represent an efficient structural method in many structural systems, such as buildings and bridges, due to additional advantages associated with the favourable redistribution of internal forces across the member and the easier satisfaction of serviceability checks. However, the design and analysis of continuous composite beams is rather complicated due to their different behaviour in positive (or sagging) and negative (or hogging) moment regions. Moreover, in regions of hogging moments, e.g. at the internal support regions of continuous members, a large part of the steel beam section is subjected to compressive stresses, thus the bottom flange and the web are susceptible to local instabilities.

In engineering practice, there are situations where composite beams are subjected to combined actions, e.g. simultaneous action of positive or negative bending and axial tension or compression. Such examples include: a) in floor beams where the axial force can either be as part of a specific bracing system or where the beam acts as part of a diaphragm [1]; b) high-rise frames where the effects of wind loading become significant and can impose large axial forces on the beams of the building; c) structures where inclined members are used, e.g. stadia beams or inclined parking ramp approaches; and d) bridges, where inclination and traffic loads may introduce large axial forces on the supporting beams.

Current structural codes, e.g. [2–4], do not provide specific rules for the design of composite beams under combined axial forces and bending moments; they rather refer to rules established for bare steel sections. Since the behaviour of a composite beam differs substantially from that of a bare steel section, the moment–axial load interaction of composite beams still deserves further investigation. Despite the large amount of available experimental data on the flexural behaviour of composite beams [5–7], experimental data on the behaviour of composite beams under combined loading is rather limited. The effects of axial tension on the sagging and hogging moment regions of composite beams were studied in previous research by the authors [8,9]. In this work, the ultimate strength of composite beams subjected to combined actions was investigated by a large experimental programme, rigid plastic sectional analyses and extensive finite element simulations. Interaction curves were established and simple design rules were proposed for

* Corresponding author. Tel.: +61 247360119.
E-mail address: g.vasdravellis@uws.edu.au (G. Vasdravellis).

0143-974X/$ – see front matter © 2012 Elsevier Ltd. All rights reserved.
http://dx.doi.org/10.1016/j.jcsr.2012.07.012

use in practice. The effect of pre-stressing on composite beams under positive bending was studied by Uy and Bradford [10] and Uy [11]. The performance of composite beams under combined bending and torsion was reported by Nie et al. [12] by studying experimentally and theoretically eleven steel–concrete composite beams. The effect of torsion on straight and curved beams was also studied by Tan and Uy [13,14]. Their research provided experimental data for the effects of torsion on composite beams with both full and partial shear connection. Based on the tests, design equations for ultimate limit analysis of composite beams were proposed. Baskar and Shanmugan [15] tested a number of steel–concrete composite girders under bending and shear loading. They found that the ultimate load carrying capacity is increased significantly compared to bare steel girders. Elghazouli and Treadway [16] presented results from a series of tests on partially-encased composite steel–concrete beam-columns. The experimental inelastic behaviour of the specimens under lateral loading and axial gravity loads was examined. The specimens in their study, however, were symmetrical through both their x and y axes and thus more appropriate for use as columns. Uy and Tuem [17] were the first to consider the effect of tension in composite beams. An analytical study on combined axial load and bending was performed through a cross-sectional analysis and a rigid plastic analysis.

This paper studies the behaviour of composite beams under the combined effects of negative bending and axial compression and is part of a large research project which aims to establish the complete interaction diagram for composite beams subjected to combined axial forces and bending moments. In this context, six full-scale tests were conducted on composite beams subjected to combined actions, while the level of the applied axial compression varied from low to high. Following the tests, a detailed nonlinear finite element model was developed and validated against the experimental results. The model was found to be capable of predicting the nonlinear response and the ultimate failure modes of the tested beams. The developed finite element model was further used to carry out a series of parametric analyses on a range of composite sections commonly used in practice. It was found that, when a compressive load acts in the composite section, the negative moment capacity of a composite beam is significantly reduced and local buckling in the steel beam is more pronounced, compromising the ductility of the section. Rigid plastic analysis based on sectional equilibrium can reasonably predict the combined strength of a composite section and, thus, can be used conservatively in design practice. Detailing with longitudinal stiffeners in the web of the steel beam in the regions of negative bending eliminate web buckling and increase the rotational capacity of the composite section. Based on the experimental outcome and the finite element analyses a simplified design model is proposed for use in engineering practice.

2. Experimental programme

2.1. Details of test specimens

Six full-scale composite beams were designed and tested as part of the experimental programme. The tested beams are denoted throughout this paper as CB1 to CB6. Specimens CB1 and CB6 were tested under pure negative moment and pure axial compression, respectively, while specimens CB2 to CB5 were tested under combined negative bending and an increasing level of applied axial compression. The relevant geometry and details of the reinforcement and shear studs are shown in Fig. 1. All specimens were constructed with a 600 mm-wide and 120 mm-deep concrete slab connected to a UB203 × 133 × 30 universal beam section. The beam-to-slab connection was achieved through 19 mm-diameter, 100 mm-long headed shear studs welded in a single line along the centre of the top flange of the steel beam. The provided number of shear studs was calculated to ensure full shear connection between the slab and the beam. The degree of shear connection in hogging moment regions of composite beams is defined as the ratio of the shear connection strength provided by the studs to the strength of the weakest component (steel reinforcement or steel beam), while the tensile strength of the slab is neglected [18]. That is:

$$\beta = \frac{N_{ss} F_{stud}}{min\{F_r, F_{beam}\}} \quad (1)$$

where β is the degree of shear connection, N_{ss} is the number of studs in the shear span (half span), F_{stud} is the strength of an individual stud, F_r is the axial strength of the reinforcement in the slab, and F_{beam} is the axial strength of the steel beam. In the experimental beams $N_{ss} = 8$, $F_{stud} = 110$ kN from the pushout tests (described later), and $min\{F_r, F_{beam}\} = F_r = 250$ kN, thus $\beta = 3.5 > 1$; therefore, a full shear connection was ensured. A group of three studs was welded to the ends of each of the beams to reduce slip and ensure full utilization of the reinforcing bars. Longitudinal and transverse reinforcement was placed in the concrete slab in the arrangement shown in Fig. 1.

Two 10 mm-thick web stiffeners were welded between the beam flanges at the point of the vertical load application to prevent premature web buckling due to the concentrated midspan load. In addition, specimens CB5 and CB6 were reinforced by using a series of web and flange stiffeners at the two ends of the beam (see Fig. 1). This configuration aimed to avoid local failure due to large stress concentration at the points of the axial load application and allowed for the high compressive loads to be partly transferred to the composite cross-section at the midspan, as will be discussed later. Due to an unexpected failure of specimen CB2 due to lateral buckling, lateral bracing was placed along the length of the beams CB3 to CB6 to eliminate the possibility of lateral–torsional buckling failure mode. The lateral bracing consisted of steel rectangular members anchored on the edges of the concrete slab and welded on the bottom (compressive) flange of the steel beam, as shown in Fig. 2.

2.2. Material property tests

Both concrete and steel material property tests were performed to obtain the actual strength of the materials. Concrete tests consisted of standard cylinder compressive tests and flexural splitting tests. The latter aimed at determining the tensile strength of the concrete. The cylinders were 200 mm high with a diameter of 100 mm, while the flexural tests were performed on 100 × 100 × 400 mm specimens. The results are summarised in Table 1. Tensile tests were also conducted on coupons cut out from the flange and web of the steel beams as well as the reinforcing bars. The values obtained from the tests for the yield stresses, the ultimate stresses at fracture, and the modules of elasticity are reported in Table 2.

The load-slip characteristics of the shear studs were evaluated by conducting three push-out tests. The push-out specimens were constructed using shear studs and concrete from the same batches as those used to form the steel–concrete composite beams in the main experimental series. Each of the push-out specimens were tested following the testing procedure described in Eurocode 4 [2]. The resulting load–slip curves showed that the average capacity of one shear stud is about 110 kN, while the maximum slip achieved during the tests varied from 8 to 14 mm, as demonstrated in Table 3. Table 3 also reports the slip values at the maximum load during the tests. These values are 5.8, 6.9, and 8 mm, demonstrating good ductility of the shear studs.

2.3. Experimental setup

A combination of load actuators was used to produce simultaneous axial compressive loads and bending moments in the composite beam specimens. The vertical load was applied with the use of a 1000 kN-capacity hydraulic actuator with a usable stroke of 250 mm. The axial compressive load was applied using four 800 kN-capacity hydraulic actuators placed in parallel. Therefore, this system was capable of applying a maximum 3200 kN axial load with a 200 mm usable

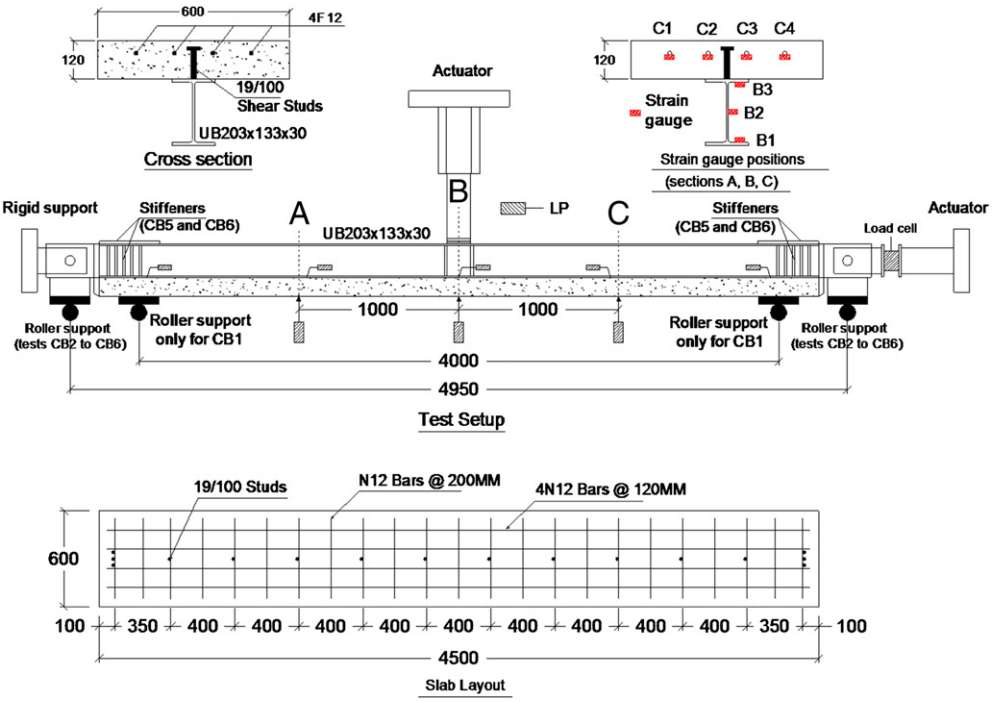

Fig. 1. Geometric details, test setup and instrumentation of the testing procedure.

stroke. The axial compressive load was transferred to the composite beam section by the use of a plate which was welded to the steel beam section and a triangular spreader plate of equal width as the beam flange, i.e. 134 mm, as schematically shown in the test setup of Fig. 1. In this way the loaded area was the area of the steel beam plus a portion of the slab area equal to the width of the spreader plate times the depth of the slab. Two roller supports at a 4000 mm-distance were used for beam CB1, which was tested under pure negative bending. For the rest of the tests, the beams were supported by the pins of the axial load applicators and roller supports placed underneath the pins, as shown in Fig. 1. The clear span for tests CB2 to CB6 was 4950 mm.

2.4. Instrumentation

A combination of linear transducers and strain gauges was deployed to record the relevant parameters and to obtain the experimental behaviour of the beams. An automatic data acquisition system was used to automatically record data from all measuring devices including load cells, strain gauges and linear potentiometers throughout the test. Strain gauges were used to measure strains of the steel beam and reinforcing bars. Strain gauges were located in sets of seven through each cross-section with one set at midspan and one set at each quarter point, as shown in Fig. 1. Linear potentiometers were used to measure the deflection of the beam. These were placed at the midspan and at the quarter points. The connector slip and interface slip were also measured by linear potentiometers. The slip was measured at the ends, quarter points and midpoint, as indicated in Fig. 1.

Fig. 2. Bracing used to eliminate lateral–torsional buckling.

2.5. Test procedure

The beam CB1 was loaded in pure negative bending; therefore it was only subjected to a vertical load. Note that, in order to facilitate the application of negative bending, the specimens were positioned with the slab underneath the steel beam, as shown in Fig. 1. The vertical load was increased until either material failure occurred or the stroke limit of the vertical load actuator was reached. In the case of specimens CB2 to CB5, vertical loading was carried out in incremental steps in the order of 10% of the theoretical design strength of the composite section. To obtain different levels of axial compression, the increments of applied axial load were varied. Both loads were increased until either material failure occurred or the maximum stroke of either of the load actuators was reached. The final beam considered, CB6, was tested in pure axial compression and only the axial loading rig was used to apply the load. During the test, a load cell was placed in contact with the steel top flange of the steel section at the midspan of the composite beam to prevent

Table 1
Material test results for concrete.

Age at testing (days)	Compressive strength (N/mm^2)	Age at testing (days)	Tensile strength (N/mm^2)
7	12	52	2.92
14	17	64	3.39
21	19	68	2.57
28	22	71	3.26
38	21	72	3.36

Table 2
Material test results for steel.

Coupon	Sample no.	Yield stress (N/mm^2)	Tensile stress (N/mm^2)	Modulus of Elasticity ($\times 10^3$ N/mm^2)
Flange	1	351	528	196
	2	357	516	179
	3	357	528	196
	4	363	523	207
	Average	357	524	195
Web	1	389	535	207
	2	391	542	203
	3	451	573	207
	4	391	537	196
	Average	406	547	203
Reinforcement	1	515	640	200
	2	517	642	201
	3	498	631	204
	Average	510	638	202

second-order bending of the beam due to the eccentricity caused by the location of the axial load applicators relative to the plastic centroid.

The resulting moment in each tested beam was calculated taking into account the equilibrium of the external forces acting on it. The following equation was used to calculate the ultimate bending moment:

$$M = \frac{p_V L}{4} + P_H e - M_{sw} \quad (2)$$

where P_V is the vertical force applied at the centre of the beam, P_H is the horizontal force, M_{sw} is the moment due to the beam's self weight and e is the eccentricity between the location of the load application pin and the plastic neutral axis of the composite beam. The eccentricity was estimated by:

$$e = \left(D_c + t_f + \frac{d_w}{2}\right) - y_c + \delta \quad (3)$$

where D_c is the slab thickness; t_f is the flange thickness; d_w is the height of the web; y_c is the depth of the plastic neutral axis (PNA), measured from the top of the slab; and δ is the measured vertical deflection at the midspan.

3. Theoretical analysis

3.1. Rigid plastic analysis

An analytical calculation of the composite beam capacities was conducted by means of rigid plastic analysis (RPA) within the section. In this analysis only the steel parts (reinforcement bars and steel beam section) of the composite section are considered to contribute to the section capacity, while the concrete in tension is neglected. Fig. 3a shows the stress distribution through the composite section as it is assumed by the RPA for the case of negative bending without axial force. For the case of axial force the plastic neutral axis is assumed to lie in several points within the section height and the resulting moment and axial compression are summed taking as centre of rotation the plastic centroid of the composite section, as shown in Fig. 3b. For comparison purposes with the experimental values, no partial safety factors were assumed and the average yield strengths resulted from the material tests were used in the calculation of the internal forces.

Table 3
Results of the pushout tests on shear studs.

Specimen	Maximum load per stud (kN)	Measured slip (mm)	
		At maximum load	At failure
PT1	102.5	5.8	8.2
PT2	112.8	6.9	13.0
PT3	106.5	8.0	14.3
Average	107.3	6.9	11.8

3.2. Finite element model

The experimental programme described in the previous sections provided data on the ultimate strength of composite beams subjected to the combined effects of negative bending and various levels of axial compression. Nevertheless, the test results regard only one specific composite section. In order to generalise the results and to consider a broader range of sections, the finite element method was employed. For this purpose, a nonlinear three-dimensional finite element model was constructed to simulate the tests on the composite beams. The model relies on the use of the commercial software ABAQUS [19]. A detailed description of the model geometry, element types, materials and solution method is given in the following sections.

3.3. Geometry and element types

The concrete slab was modelled using eight-node linear hexahedral solid elements with reduced integration, namely C3D8R in ABAQUS, while the steel beam was modelled with eight-node elements with incompatible modes (C3D8I). The main reason for using different elements is that the elements with incompatible modes are efficient to capture local instabilities such as flange and/or web buckling without the need to introduce imperfections in the model. The reinforcing rebars were modelled as two-node three-dimensional linear truss elements, T3D2. The fly bracing was modelled indirectly by applying boundary conditions which prevent lateral displacement at the same points on the beam compression flange as the fly bracings were located in the tests. Due to the symmetrical geometry and loading, only half of the beam was modelled, while appropriate boundary conditions were applied to the plane of symmetry. An overview of the mesh and a schematic representation of the various modelling assumptions are depicted in Fig. 4.

3.4. Interactions

To model the reinforcement in the slab the embedded element technique was employed. The embedded element technique in ABAQUS is

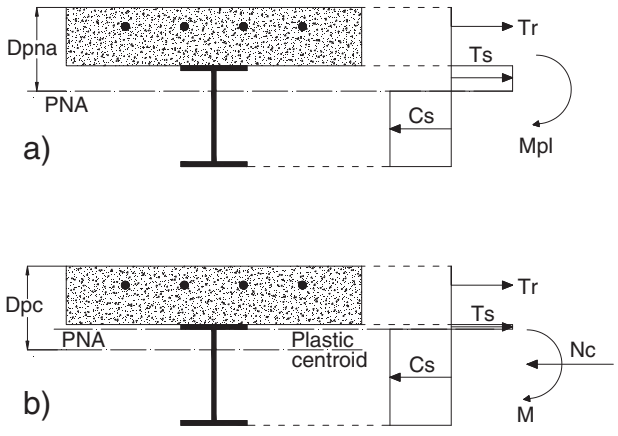

Fig. 3. Stress distribution according to RPA: a) pure negative bending; and b) assumed stress distribution resulting to axial compression and negative moment in the section (PNA = plastic neutral axis).

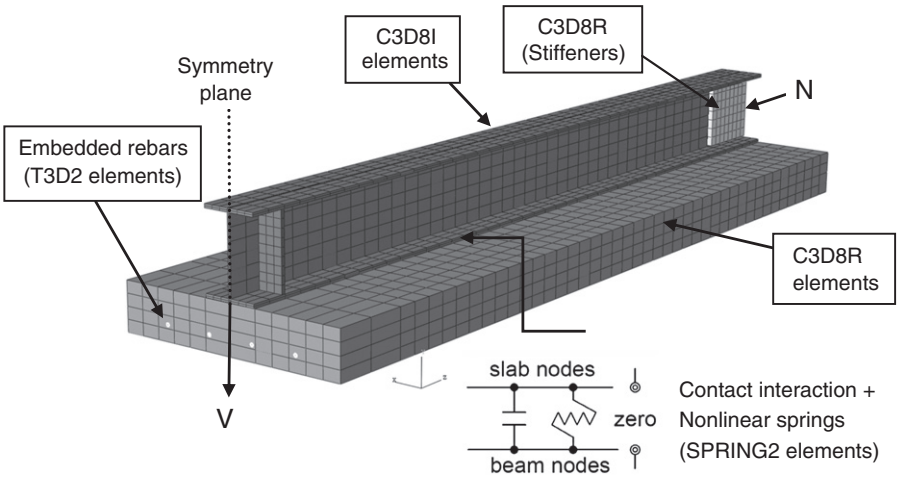

Fig. 4. Details of the finite element mesh used for modelling the composite beams.

used to specify an element or a group of elements that lie embedded in a group of host elements whose response will be used to constrain the translational degrees of freedom of the embedded nodes. In the present case, the truss elements representing the reinforcement are the embedded region while the concrete slab is the host region. Using this technique, it is assumed that perfect bond exists between the rebars and the surrounding concrete. In addition, a contact interaction was applied in the beam–slab interface which did not allow separation of the surfaces after contact in order to prevent uplift. The node-to-surface contact with small sliding was used while the "hard" contact without friction was specified as the contact property.

3.5. Material properties

The stress–strain relations obtained from material tests were converted into piecewise linear curves and used to model the steel material for the beam and the reinforcing bars, as illustrated in Fig. 5. A plastic material with isotropic hardening law was used as the constitutive law for all the steel parts of the model.

The concrete material stress–strain relationship was calibrated according to the values obtained from the concrete cylinder and splitting tests. The stress–strain curve for compression followed the formula proposed by Carreira and Chu [20], while the tensile behaviour is assumed to be linear up to the uniaxial tensile stress provided by the material test. The stress–strain law used is plotted in Fig. 5a. The post-failure behaviour for direct straining across cracks is modelled using the tension-stiffening option and determining a linear relation until stress is zero at a strain value of 0.05. This value is used to avoid numerical instabilities in the computational procedure while accuracy is not affected considerably. There are two plastic models available in ABAQUS for modelling the concrete behaviour. In the present analysis the damaged plasticity model was preferred over the smeared cracked model. This model provides a general capability for the analysis of concrete structures under static or dynamic and monotonic or cyclic loading based on a damaged plasticity algorithm. Compared to the companion model (smeared crack model), it models concrete behaviour more realistically but it is computationally more expensive. Nevertheless, this model was chosen for monotonic loading due to its numerical efficiency when full inelastic response has to be captured.

A discrete spring model representation of shear studs is chosen to simulate the slip in the slab–beam interface. The nonlinear spring element SPRING2 was adopted to connect a beam flange node with a slab node at the interface at the same positions where studs were welded to the specimen, as schematically shown in Fig. 4. The force slip law for the spring element is derived by the standard push-out tests on 19 mm-diameter shear studs. A piecewise linear curve was fitted to the experimental diagram and defined as the force-slip law for the springs, as shown in Fig. 5d.

3.6. Loading and solution method

The vertical load was applied as an imposed displacement on the top of the beam flange, while the axial load was applied as an edge pressure on the steel beam section. The axial load direction was kept constantly horizontal, i.e. it did not follow the rotation of the edge, in order to be consistent with the experimental loading procedure. The analysis consisted of two steps. In the first step the contact interactions were established, ensuring that numerical problems due to contact formulation will not be encountered during the next steps, while in the second step the vertical and the axial loads were applied simultaneously, following the experimental procedure. The static nonlinear solution algorithm with adaptive stabilisation as a fraction of dissipated energy was employed to solve for the nonlinear response of the composite beams. Finite element analysis with concrete elements in tension may result in convergence problems. To avoid these, the discontinuous analysis option was also used in the general solution control options.

3.7. Failure criteria

The behaviour of the finite element model and the failure modes at the ultimate deformation of the composite beams were monitored during the FEM analyses through the establishment of specific failure criteria which were defined corresponding to the ultimate strength of the various section components. In particular, failure of the composite beam in the simulation was identified by one of the following situations: a) flange or web buckling, b) reinforcement fracture, and c) shear connection failure. While local instabilities can be captured accurately using the large displacement nonlinear analysis option in ABAQUS, the second and third conditions should be identified by monitoring some specific response quantities. The strain of the reinforcing bars and the relative displacements in the nonlinear springs representing the studs were monitored during the analysis. An excessive strain in the rebars reaching the experimental rapture values should indicate a reinforcement fracture, while a measured slip near or above the failure slip of the push-out tests was a criterion for shear connection failure. Finally, a ductile failure mode was defined when none of the above criteria was met and the analysis was ended by numerical problems due to excessive cracking of concrete in tension, while the ultimate load achieved was easily identified by the load–deflection curve.

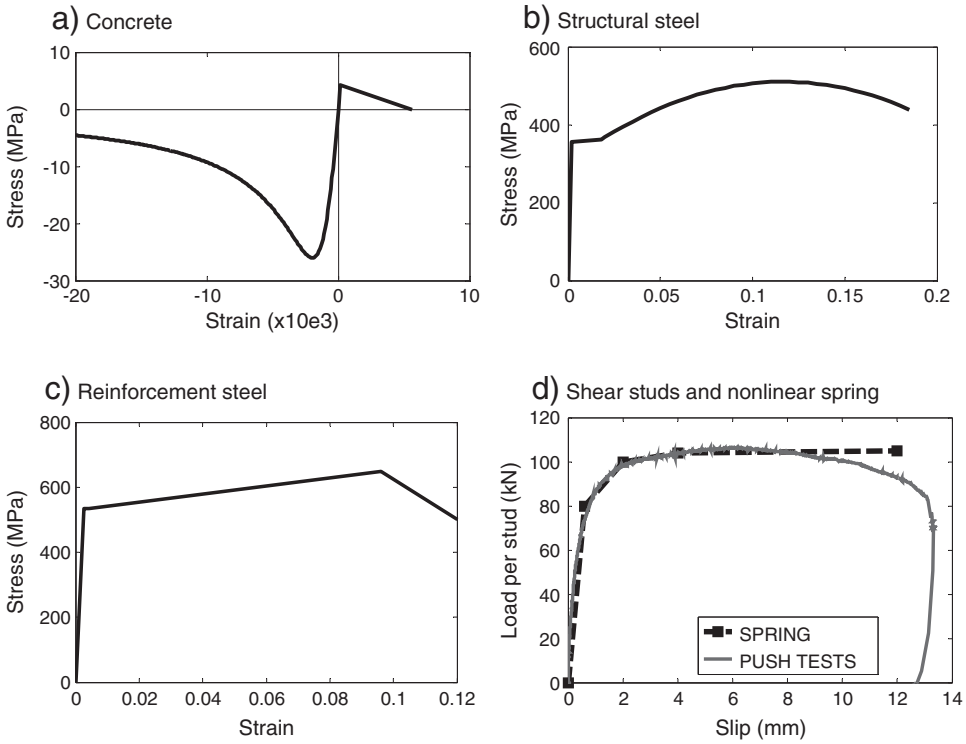

Fig. 5. Material stress–strain laws adopted in the finite element model a) concrete, b) structural steel parts, c) reinforcement, and d) shear stud force-slip law.

4. Results and discussion

4.1. Observations and failure modes

Table 4 summarises the failure modes and the ultimate strengths achieved by the six composite beams. The ultimate pure moment and axial capacities achieved during the tests are denoted as M_u and N_u, respectively. The applied axial compression levels to specimens CB2, CB3, CB4 and CB5 were equal to 11, 32, 46, and 80% of the maximum compressive load applied in composite beam CB6, respectively. The corresponding reduction in negative moment capacity was 25, 11, 29, and 80% with respect to M_u.

The common failure mode of all specimens was the local buckling in the compressive parts of the steel beam. However, the simultaneous action of a compressive force accelerated the local buckling failure in beams CB2 to CB5. Specimen CB1 failed due to local buckling at the midspan region, as shown in Fig. 6a. The local failure initiated from the web of the steel section and propagated to the compressive flange. Significant cracking of the slab was observed at the same region, as shown in Fig. 6c. The failure mode of specimen CB2 was similar to that of specimen CB1, and the axial compression load equal to 256 kN (or 11% of N_u) introduced in that specimen reduced the moment strength of the beam from −186 to −140 kNm, or 25% reduction with respect to M_u, as it is shown in Table 4. Specimens CB3 and CB4 were loaded with moderate and relatively high axial compressive forces (32 and 46% of N_u, respectively) and the reduction in negative moment capacity was significant, assuming values 11% and 29% of M_u, respectively. Local buckling in these beams was observed in the region immediately before the transverse stiffeners at the midspan, as depicted in Fig. 6b. A very high compressive load, equal to 80% of N_u, was introduced in specimen CB5 and the reduction in moment capacity was 80% of M_u. Local failure in this specimen was observed at the region immediately after the end of the flange reinforcing plates, where the negative moment was maximum. The same failure mode was observed for specimen CB6, which was loaded under axial compression only; the buckling took place at the region immediately after the reinforcing plates, as shown in Fig. 6d. In addition, significant cracking in the slab at the point of the axial load application was observed at the end of the test.

During the test of the beam CB5, when a high axial compression load was applied in the composite section with no additional stiffeners at the ends of the beam, the steel beam buckled immediately after the axial load application point at a compression force slightly lower than the plastic axial capacity of the steel beam, i.e. 1334 kN. After the installation of the additional web and flange stiffening plates at the anchorage regions, a considerable increase of the compression capacity of the steel beam was observed, as evidenced by the values of Table 4. This increase in compression capacity was about 41% (from 1334 kN to 2257 kN). Therefore, in order to transfer substantial compressive forces in a composite beam without experiencing premature buckling of the steel section, reinforcing the flanges and the web with additional plates is recommended.

Table 4
Failure modes and experimental ultimate strengths of composite beams.

Specimen	Loading	Failure mode	Ultimate moment (kNm)	Axial force (kN)
CB1	Pure negative bending	Ductile	−186 (M_u)	0
CB2	Negative bending axial compression	Local buckling	−140 (−25%)[a]	256 (11%)[b]
CB3	Negative bending axial compression	Local buckling	−166 (−11%)[a]	718 (32%)[b]
CB4	Negative bending axial compression	Local buckling	−132 (−29%)[a]	1048 (46%)[b]
CB5	Negative bending axial compression	Local buckling	−38 (−80%)[a]	1801 (80%)[b]
CB6	Axial compression only	Local buckling	−11	2257 (N_u)

M_u: ultimate negative moment resistance and N_u: Ultimate compression load applied.
[a] Reduction with respect to M_u.
[b] Percentage of maximum applied axial compression.

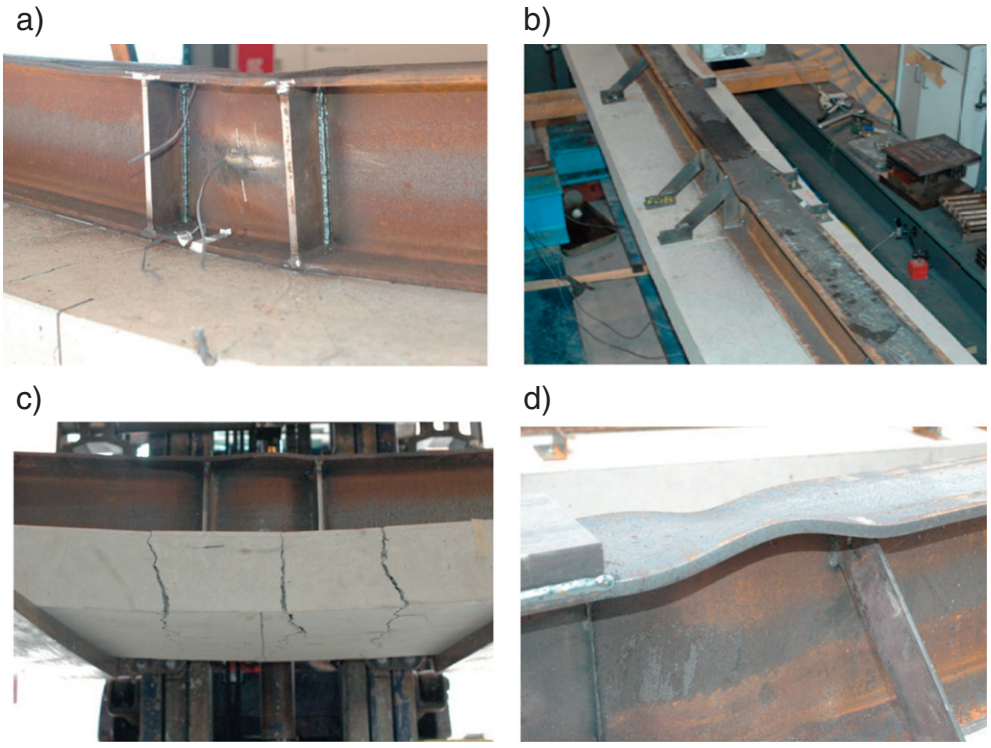

Fig. 6. Typical failure modes of the specimens: a) local buckling in the web of CB1; b) flange buckling (CB2); c) cracking of the concrete slab; and d) failure of specimen CB6 immediately after the reinforcing plates.

4.2. Force-deformation behaviour

Fig. 7a plots the normalised moment versus midspan deflection response of specimen CB1 along with the FEM model prediction. The recorded moment is divided by the theoretical negative plastic moment resistance, M_{pl}, resulting from the RPA. The specimen sustained a maximum force equal to 186 kN, which is equal to the achieved moment, and a maximum midspan deflection equal to 120 mm. Note that the experimental moment resistance is 20% higher than the resistance predicted by the RPA. This is attributed to the considerable strain hardening of steel which normally occurs during a test. The moment–deflection curve softens after the peak load and it starts to descend at a deflection equal to 100 mm indicating the initiation of inelastic local buckling in the compressive parts of the steel beam. The failure mode of specimen CB1, however, can be characterised as ductile, since local buckling initiated after the full plastic resistance was developed and considerable rotation capacity was achieved.

Experimental and theoretical normalised axial compression versus axial displacement curves for the beam CB6 are plotted in Fig. 7b along with the FEM model prediction. The force is divided by the axial compressive strength of the beam, N_p, equal to the product of the steel beam area and the nominal yield strength of steel. Note that the experimental curve plots the total stroke displacement as recorded by the actuator against the total axial force in the steel beam and, thus, it does not include any possible local flexibilities or minor local yielding effects which can reduce the stiffness. In effect, the initial stiffness of the experimental curve is significantly smaller than the numerical one, which is attributed to the aforementioned flexibilities. Both the FEM analysis strength prediction and the test strength are considerably higher than N_p, with the difference being 62 and 69%, respectively.

4.3. Interaction diagram

Fig. 8 plots the negative moment versus axial compression interaction diagram resulted from the experimental procedure along with the results from the theoretical analyses. From the experimental data points, it can be concluded that the negative moment capacity of a composite beam is reduced when an axial compressive load acts simultaneously to the section.

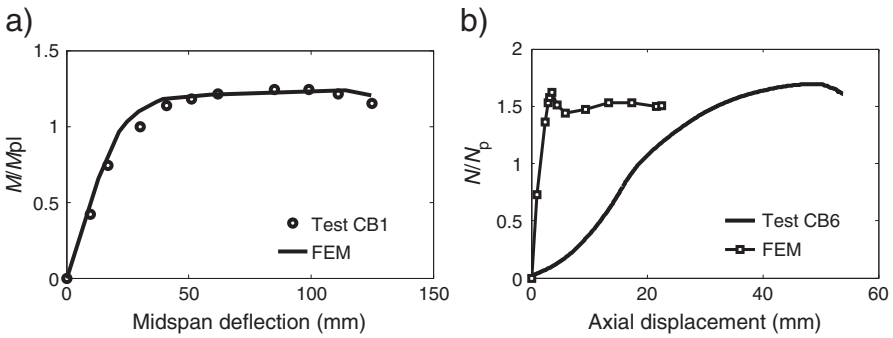

Fig. 7. a) Normalised moment versus midspan deflection response of CB1; and b) axial compression versus axial displacement response of CB6.

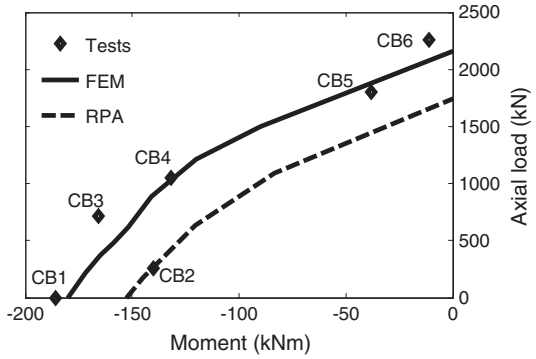

Fig. 8. Negative moment versus axial compression interaction diagrams resulting from the tests and the theoretical analysis.

This reduction is observed even when low axial loads are present. However, a significant reduction of the moment capacity of specimen CB2 is observed, although this specimen was loaded under a relatively low axial compressive force (256 kN). Specimen CB2 has failed prematurely due to lateral buckling before reaching the section's ultimate moment capacity. For this reason, the fly bracing was included for the subsequent tests. The combined strength of this specific specimen appears to decline considerably from the trend observed from the values of the other specimens and from the RPA. It is the authors' opinion that this value is not representative of the actual interaction diagram. The curves of both the RPA and the experimental values follow a similar shape after neglecting the premature failure of specimen CB2. The experimental study has confirmed that sectional rigid plastic analysis is a reasonable yet conservative assumption of the ultimate design strength of composite beams under the effects of combined negative bending and axial compression. The plastic resistances resulting from the RPA lie well below the experimental capacities. Therefore, rigid plastic analysis can be used for the design of composite beams subjected to combined forces since it is reasonably accurate and will produce a conservative estimation for composite beam strength under the combination of negative bending and axial compressive force.

4.4. FEM model validation

In order to validate the accuracy of the finite element model to predict the combined ultimate strength, the experimental loading of the beams was reproduced in the FEM analyses. The extreme cases of pure negative bending and pure axial compression were first simulated followed by the combined loading cases. Fig. 7a shows that the FEM model is in very good agreement with the experimental force–deflection curve of specimen CB1, both in terms of initial stiffness and ultimate moment capacity. The stiffness and negative moment strength predicted by the model are 7.2 kN/mm and −182 kNm, respectively, which are very close to the experimental values of 6.8 kN/mm and −186 kNm. In addition, the failure mode experienced by the FEM model is the local buckling of the beam compressive flange and the web, which initiated after the development of the full plastic moment resistance in the composite beam section, as occurred in the test. This can be verified by the initiation of the descending part of the curve in Fig. 7a, while the deformed configuration in Fig. 9a depicts the buckling in the composite section at the ultimate deformation which is consistent with the experimental deformed shape in Fig. 9b. The model predicts reasonably accurate the axial compressive strength of the composite section, since it predicts an ultimate value of 2164 kN, which is about 4% lower than the experimental one (2257 kN).

Fig. 8 shows that the FEM model predicts well the ultimate strength of composite beams when simultaneous negative bending moment and axial compression act to the section. The resulting FEM interaction points are in very good agreement with the corresponding points from tests CB1, CB4, CB5 and CB6, while the experimentally calculated combined strength of specimen CB3 is 8% higher than the FEM prediction. The combined strength of specimen CB2 is 40% lower than the FEM predictions for the reasons outlined in the previous section. The shape of the interaction resulting from the FEM analyses verifies the assumption that the excessively low strength of specimen CB2 is not representative of the actual moment–compression interaction relationship of the composite section if lateral buckling is precluded. In addition, some variability in the ultimate strength results between the tests and the numerical model is considered reasonable and can be attributed to the following reasons: a) variability in material properties, which is present even for specimens made of the same batch, as can be verified by the material tests values of Table 2; and b) the calculation of the experimental strength which is based on the use of Eq. (1) and estimation of the depth of the plastic neutral axis. Although this estimation was based on consistent criteria for all tests, some uncertainty still exists. For the determination of the eccentricity and, thus, the secondary moment generated by the axial load, a back-calculation procedure was used, i.e. the depth of the plastic neutral axis was calculated based on the FEM model stress distribution for a given level of applied axial compression. The shape of the interaction curves resulting from the RPA and the FEM model are in very good agreement, with the higher strength predicted by the ABAQUS model being ascribed to the strain hardening and tension stiffening effects introduced in the material properties. Considering the complexity of the experimental setup and the uncertainties associated with the interpretation of the results, it can be concluded that the FEM model can capture the actual behaviour with good accuracy and can be used for further studies on the behaviour of composite beams under combined loading.

5. Parametric studies

5.1. Parametric beam designs

The finite element model presented in the previous section was validated against the experimental data and was proved to be reliable and accurate to capture the ultimate strength of composite sections under the combined effects of axial compression and negative bending. In order to generalise the results and to propose a reliable interaction equation for design, a parametric study was conducted on a series of beam sections commonly used in engineering practice. In the parametric study the span length was varied and, accordingly, the slab effective width and reinforcement ratio were designed for each parametric case according to the current structural codes.

The design example is taken as a two span continuous beam, as shown in Fig. 10. It is assumed that the beam is part of a grid consisting of beams in 2 m distance to each other and with roller supports at the external points. A 120 mm slab is assumed to act compositely with the steel sections, thus the beams to be designed are two-span continuous composite beams. It is assumed that the dead load of the structure is $DL = 4.0$ kN/m^2 and the live load is $LL = 5.0$ kN/m^2. The ultimate limit state (ULS) design load combination is taken according to Eurocode 1 as $q_{des} = 1.35 * DL + 1.5 * LL$, giving a design load of 25.8 kN/m on each internal beam. The moment in the middle support is equal to $M_{des} = -0.125 q_{des} L^2$ while the shear force is equal to $V_{des} = 1.25 q_{des} L$, where L is the span length. The composite beam section under consideration is the section under negative moment at the middle support of length L_e indicated in Fig. 10. For the parametric study, the span length L values range from 6 m to 20 m with a step of 2 m. By varying the span length, the effective width of the slab, b_{eff} (defined according to Eurocode 4 [2]), is also affected, ranging from 0.75 m for the 6 m span length and assuming a maximum value of 2 m. The reinforcement in the slab, A_s, consists of 12 mm-diameter bars at 150 mm distance to each other. A summary of the parametric beam designs is given in Table 5. For comparison reasons, the steel sections are given in both European shapes (IPE) and Universal Beam shapes (UB), although the IPE sections are used in the finite element analyses. Also presented in

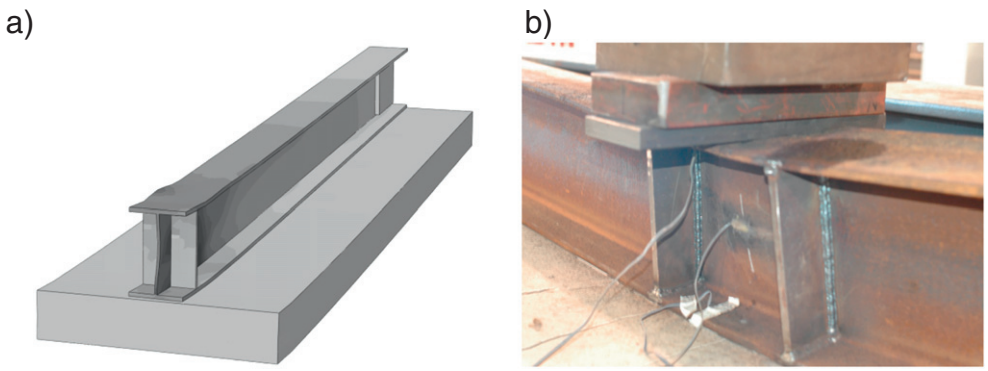

Fig. 9. Local buckling in the flange and web of the beam a) during the test, and b) as captured by the FEM model.

Table 5 are the moment and shear utilization ratios, the shear stud number and spacing needed to achieve a full shear connection degree employing 16 mm-diameter studs, and the slenderness ratios of the web of the steel beams, d_w/t_w. Since the design shear force is lower than the 50% of the plastic shear resistance of the steel section, the shear–moment interaction effects are neglected in the design (plastic moment resistance is not reduced due to shear force effects), according to Eurocode 3 [21]. The beam considered in the FEM analyses is a simply supported beam of length L_e loaded at the midspan (simulating the force from the support). Only half of the beam was modelled ($L_e/2$) and appropriate boundary conditions were used at the symmetry plane to exploit the symmetric geometry and loading conditions.

5.2. Interaction diagrams

All the parametric beams were subjected to combined negative bending moment and axial compression. First, a pure moment and a pure axial load analyses were performed. After that, the model was subjected to a constant vertical load at the midspan and various levels of axial compression acting simultaneously, ranging from 0.1 to 0.8 of the theoretical ultimate axial resistance of the steel section. The compressive load was applied in the same way as was applied in the experimental setup, i.e. in the steel section and a portion of the slab equal to the width of the beam flange. The analysis was continued until one of the failure criteria described previously was met.

Fig. 11 shows a comparison of the negative moment versus compressive axial force interaction diagrams between the results of the finite element analyses and the RPA for the parametric beams. The

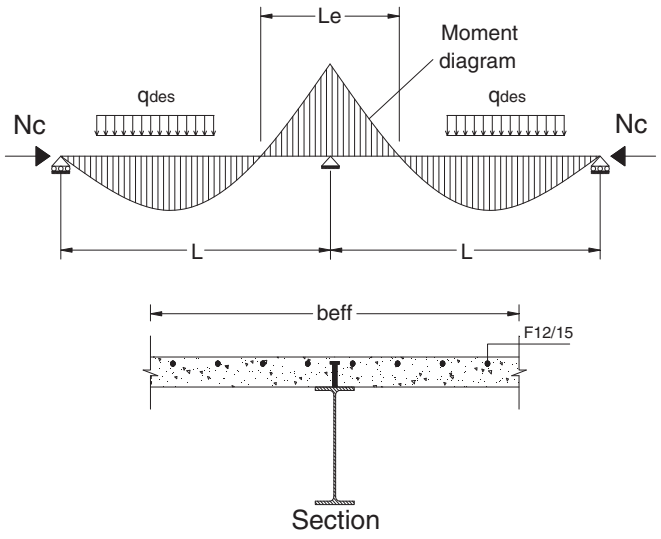

Fig. 10. The design example.

main observation is that the interaction diagrams follow the same trend in both analyses, although the bending and combined strengths resulting from the FEM model are in general greater than the corresponding resistances predicted by the RPA. This outcome was expected due to the hardening behaviour introduced in the material constitutive model of the steel material. It can be concluded from the parametric study that the RPA gives conservative results for the combined strength of composite beams and can be safely used in structural design.

Fig. 12 plots the interaction data points resulting from the FEM analyses for the eight parametric beams in the same graph. The main outcome is that the bending strength of a composite beam is reduced under the presence of a compression force. In most of the composite beams, this reduction is observed even under low axial loads, although it is more pronounced when axial compression takes moderate and large values. However, for the largest parametric sections, i.e. for the IPE500 and IPE600, the FEM results show that the moment capacity is not significantly affected or is slightly increased under the effects of a low axial compression force, while for the shorter sections the moment capacity is immediately reduced.

The common failure mode of the parametric beams was the local buckling at the midspan region. Typically, web buckling was the prominent failure in beams under negative bending, while the introduction of a compressive force resulted in an earlier failure and the ultimate deformation included in some cases the simultaneous development of flange and web buckling. This is a reasonable outcome, since the imposed force combined with the negative moment introduce immediately high compressive stresses in the bottom flange of the composite beam. Under pure compressive loading, all the parametric beams failed due to instabilities in the steel beam that arose immediately after the end of the reinforcing plates near the load application point. The typical failure modes of the parametric beams are shown in Fig. 13 for the IPE360 section. The failure modes of the numerical models generally confirmed the observed failure modes during the experimental testing.

5.3. Detailing to eliminate local buckling

In composite beams under negative bending the plastic neutral axis is shifted towards the slab and, thus, a larger portion of the steel web is under compressive stresses, as shown in Fig. 14a, which makes the steel section more susceptible to local buckling phenomena. Indeed, as described in the previous section, all parametric beams have failed by local buckling in the compressive parts. For this reason, it is recommended [18,22] that the web should be classified taking into account the distribution of the stresses through its height. According to Eurocode 3 [21] the parametric beam sections in this study are classified as Class 1 for bending, which means that they are able to develop the full plastic moment and adequate rotation capacity before failure. However, if the actual distribution of stresses through the composite section under negative bending and axial compression is taken into account, the webs are classified as Class 2

Table 5
Details of the parametric beam designs.

L (m)	q_{des} (kN/m)	M_{des}/M_{pl}	V_{des}/V_{pl}	b_{eff} (mm)	A_s (mm^2)	Beam section	Shear studs (N_{ss}/spacing in mm)	d_w/t_w
6	25.8	0.65	0.37	750	565	IPE240 (UB254×102×28)	8/428	38
8	25.8	0.71	0.36	1000	753	IPE300 (UB305×165×40)	12/363	43
10	25.8	0.72	0.33	1250	942	IPE360 (UB356×171×57)	14/384	46
12	25.8	0.81	0.32	1500	1130	IPE400 (UB457×152×60)	18/411	50
14	25.8	0.84	0.33	1750	1318	IPE450 (UB457×152×82)	16/400	47
16	25.8	0.85	0.31	2000	1507	IPE500 (UB457×191×98)	22/380	51
18	25.8	0.86	0.29	2000	1695	IPE550 (UB533×210×109)	24/391	52
20	25.8	0.86	0.28	2000	1883	IPE600 (UB610×229×125)	26/400	53

or 3, which means that they may not be able to develop the full plastic moment or they do not possess sufficient rotation capacity and, thus, they are not suitable for global plastic analysis of a structure.

Fig. 14b shows the typical failure mode of a composite beam in ABAQUS after the development of web buckling. Typically one and a half half-waves were formed near the midspan region in the symmetric model, as shown in the same figure, thus three half-waves should be formed at the midspan region of the whole beam. Based on the parametric beam analyses, the average distance between the point of maximum lateral deflection in the web of the beam and the internal edge of the compressive flange was equal to about $0.375\times D_b$, where D_b denotes the beam depth, regardless of the presence or not of a compression force. In addition, the length of the disturbed region, i.e. the length of the three half-waves, was measured and its variation in the parametric analyses is plotted in Fig. 15 as ratio of wave length, L_w, to beam depth, D_b. It is observed that the length of this region in the symmetric model in all the parametric sections is about equal to the beam depth, thus the length in the whole beam should be two times the beam depth.

Elastic or inelastic local buckling does not represent a catastrophic failure mode due to the significant post-buckling reserve that steel sections commonly present [18], although it considerably compromises the rotation capacity, or ductility, of a section. The local buckling performance of a web plate in bending and axial compression can be improved by placing longitudinal stiffeners parallel to the direction of the longitudinal stresses. The use of transverse stiffeners is not adequate to resist web buckling unless they are placed in distances $s \ll D_b$ [23,24]. This is verified in the tests, where the transverse stiffeners placed in the midspan (see also Fig. 1) did not prevent the inelastic local buckling in the flange and/or web.

Design rules are proposed in this section for the detailing of the longitudinal stiffeners in the midspan regions of composite beams under combined negative bending and compression. Based on the results of the FEM parametric study, it is reasonable to assume that the optimal position of the compressive flange, d_s, measured from the internal edge of the compressive flange, and the length of a longitudinal stiffener, L_s, are:

$$d_s = 0.375 \times D_b \tag{4}$$

$$L_s = 3 \times D_b. \tag{5}$$

Note that despite the value of $2\times D_b$ recorded for the length of the disturbed region, the value $3\times D_b$ is recommended for providing a margin of safety in the midspan region.

Fig. 14a illustrates the position of the longitudinal stiffener at the symmetric beam. In addition, the longitudinal stiffener should have sufficient stiffness in the direction of the plate buckling, i.e. transverse to the web plane, to remain straight and, thus, prevent the lateral displacement of the web plate. To the knowledge of the authors, current standards do not provide explicit rules for the determination of the necessary moment of inertia, I_s, that a longitudinal stiffener should possess. For composite beams under negative bending and axial compression,

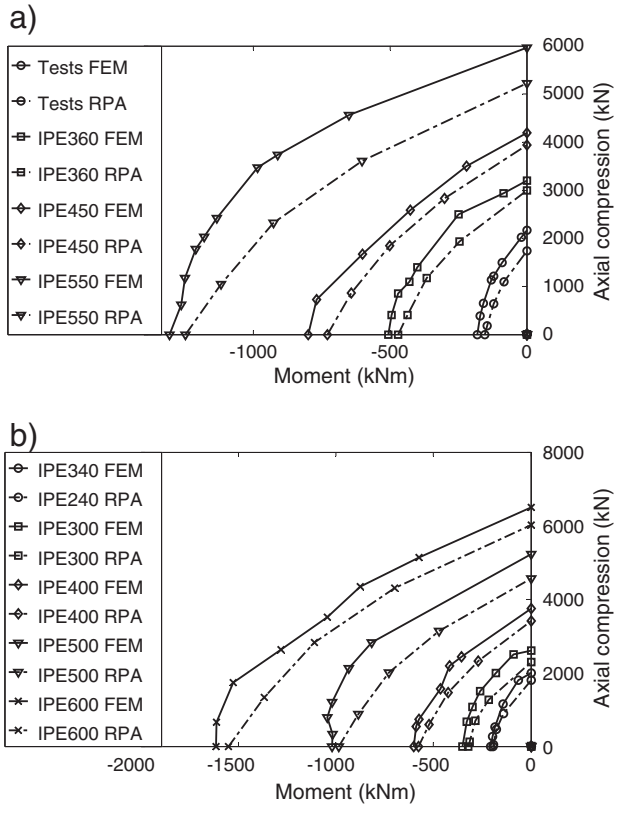

Fig. 11. Interaction diagrams resulting from the FEM analyses on the parametric beam sections.

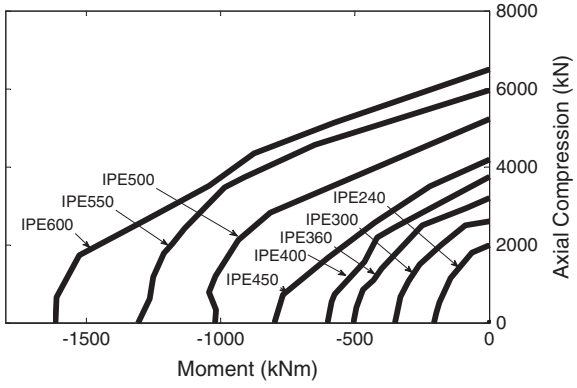

Fig. 12. Comparison of interaction diagrams resulting from the FEM for all parametric beams.

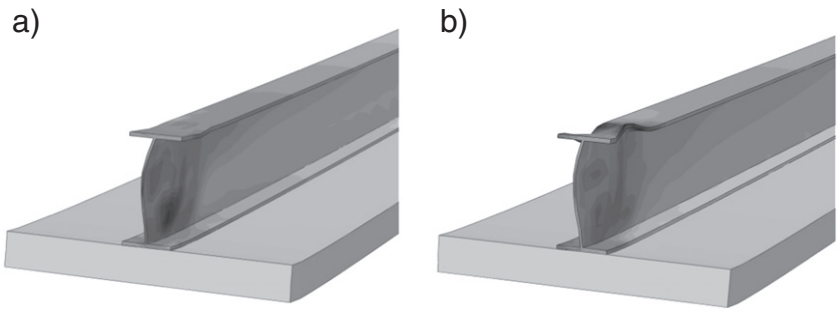

Fig. 13. Failure modes in the IPE360 parametric section: a) under negative bending; and b) under combined bending and compression.

the value recommended by the Australian Standards for steel structures, AS4100 [25], is herein adopted:

$$I_s = 4d_w t_w^3 \left[1 + 4\frac{A_{st}}{d_w t_w}\left(1 + \frac{A_{st}}{d_w t_w}\right)\right] \quad (6)$$

where A_{st} is the area of the longitudinal stiffener section, and d_w and t_w are the depth and thickness of the beam web, respectively. Note that, at least in the parametric sections, to satisfy this stiffness criterion it is required that longitudinal stiffeners be placed in both sides of the web, as mentioned in Fig. 14a.

To check the effectiveness of the proposed design details, the aforementioned geometric characteristics of the longitudinal stiffeners were incorporated in the FEM models and the analyses were repeated for all the parametric sections. Fig. 16 shows the deformed shape of three selected sections with and without longitudinal stiffeners. The proposed detailing eliminated the local buckling phenomena in the compressive parts of composite beams. This is also evidenced by the resulted force versus deflection curves, which are plotted in Fig. 17 for the same sections. The use of longitudinal stiffeners at the midspan region with the proposed geometric details enhanced the rotation capacity of the composite sections.

6. Proposed design equations

Based on the experimental results and the FEM parametric analyses, a simplified equation for the design of composite beams under

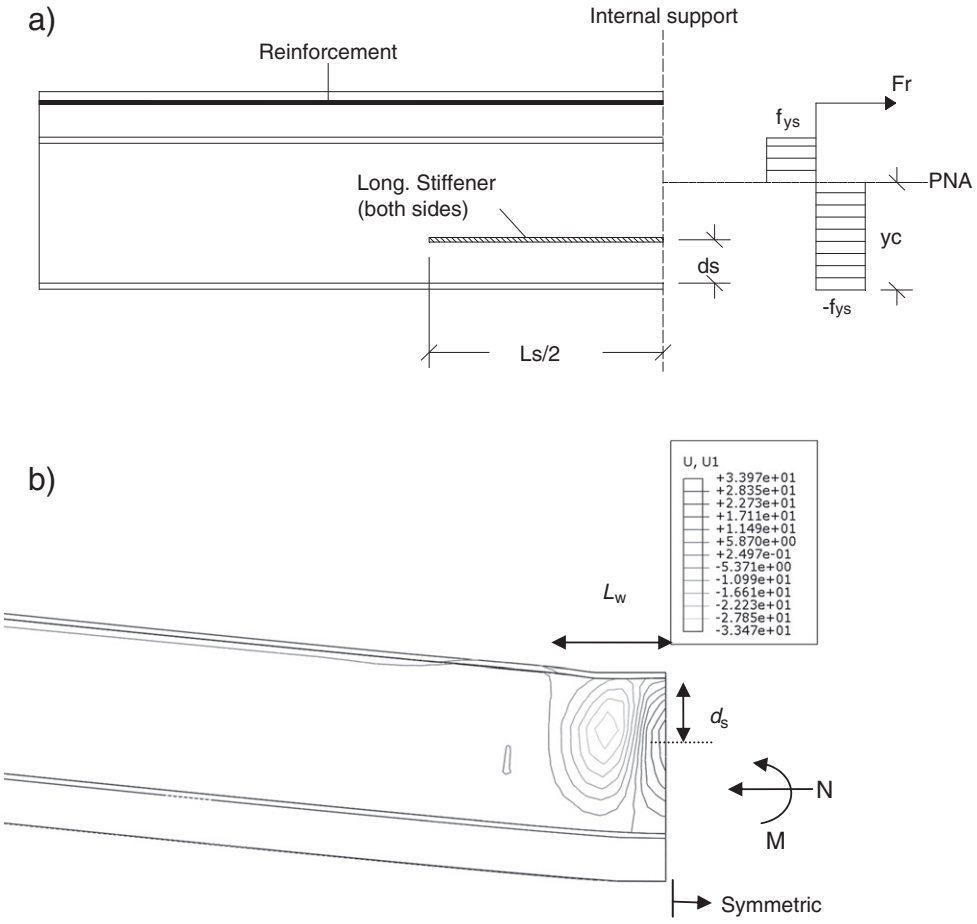

Fig. 14. a) Proposed position and length of longitudinal stiffeners; and b) web buckling in composite beam (isoline plot of deflection transverse to the beam web).

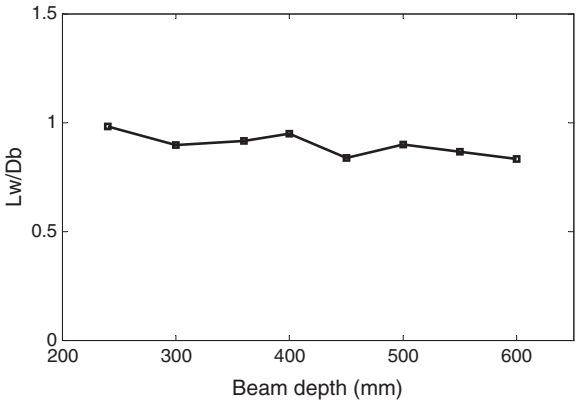

Fig. 15. Variation of the buckled region length to beam depth ratio in the parametric beams.

negative bending and axial compression is proposed in this section. The interaction data points resulting from the parametric study are plotted in non-dimensional form in Fig. 18. This is done by dividing the acting moments and axial forces by the corresponding plastic resistances of the sections. In the same graphs, the design equation is superimposed and denoted as "Design". The following equation is proposed for the interaction of negative bending moment and axial compression in a composite beam:

$$\frac{M}{M_u}+\frac{N}{N_u}\leq 1.0 \tag{7}$$

where M_u and N_u are the negative moment and axial compression plastic resistances of the composite section, respectively. According to this formula, the hogging moment resistance of a composite beam is reduced with the presence of compression forces following a linear relationship. It is noted that, although the interaction diagrams from the parametric analyses indicated that in some cases the reduction in moment capacity is delayed (see Fig. 12), a linear reduction is proposed for a reasonably conservative design, which also conforms with the experimental output. The proposed design formula assumes that adequate lateral restrain is provided to the compression flange so that flexural or distortional buckling are excluded as failure modes. In addition, longitudinal stiffeners according to the design details proposed in the previous section is recommended to be welded to the steel beam web at the internal support regions of continuous composite beams to ensure that web local buckling is delayed and adequate rotation capacity for plastic structural analysis is available.

7. Conclusions and further research

This paper presented the results of an extensive experimental and numerical investigation that was carried out in order to study the effects of axial compression on the negative moment capacity of steel–concrete composite beams. The experiments permitted the construction of an interaction curve located in the first quadrant of the complete moment–axial load interaction diagram. Rigid plastic sectional analyses and nonlinear finite element models were employed to provide further

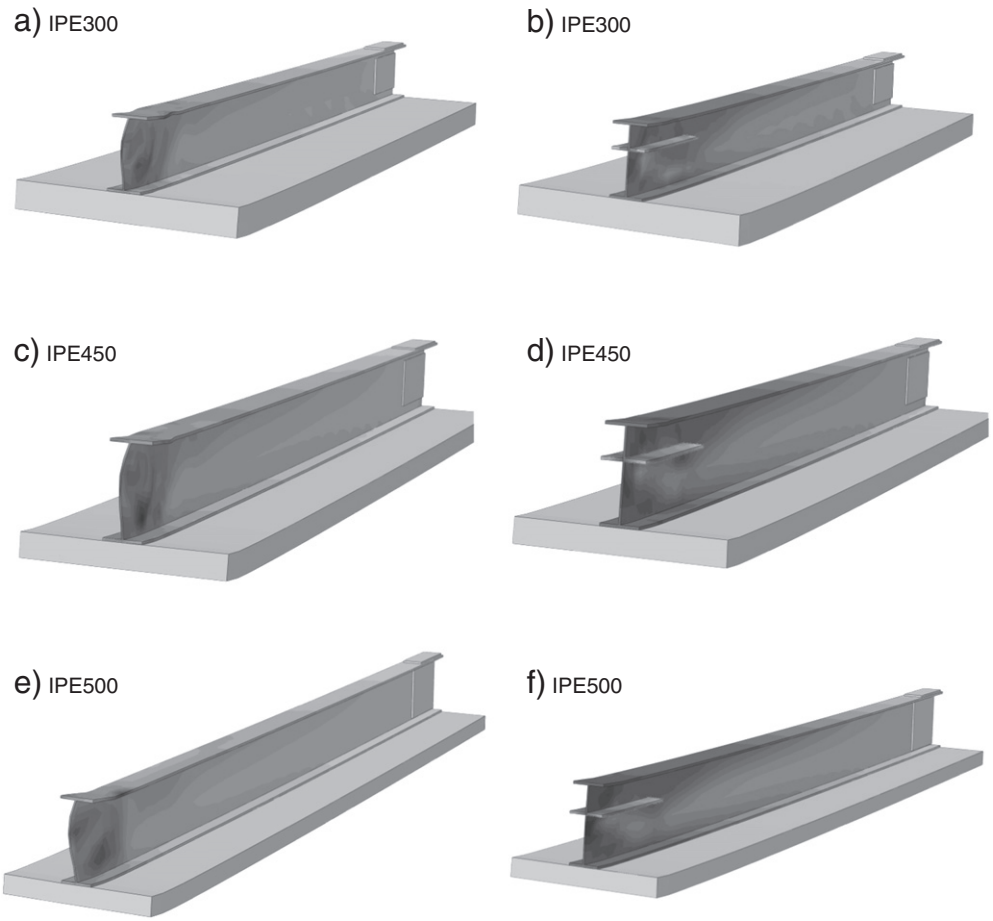

Fig. 16. Deformed configuration of three selected sections with and without longitudinal stiffeners (darker regions indicate larger stress concentrations but not necessarily yielding).

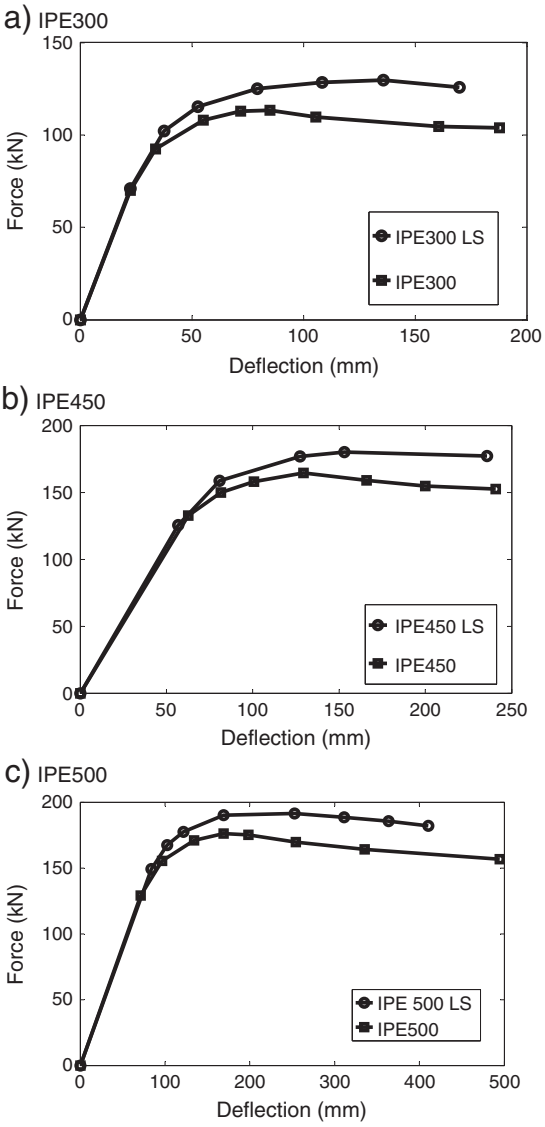

Fig. 17. Applied load versus midspan deflection of three selected sections with and without longitudinal stiffeners.

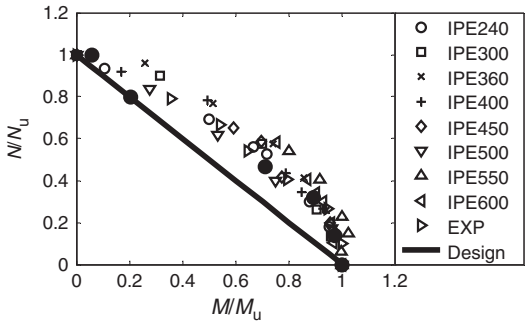

Fig. 18. Non-dimensional form of the interaction diagrams and proposed design equation for the design of composite beams under combined axial compression and negative bending moment.

insight on the behaviour of composite beams and to extend the results to a range of steel sections commonly used in engineering practice. Based on the experimental and numerical results presented herein the following conclusions are drawn:

- Experimental testing and numerical simulations demonstrated that the negative moment capacity of a composite beam is significantly deteriorated under the simultaneous action of an axial compressive force.
- Compressive loading accelerates local buckling failure modes in the compression zones of a composite section and compromises its rotation capacity.
- In order to transfer substantial compressive forces in a composite beam without experiencing premature buckling of the steel section, reinforcing the flanges and the web with additional steel plates locally at the edges is recommended.
- Rigid plastic analysis can be conservatively used for the design of composite beams under combined negative bending and axial compression.
- The developed three-dimensional nonlinear finite element model can be used as a tool for the assessment of the nonlinear behaviour and the ultimate failure modes of composite beams under combined negative bending and axial compression.
- Longitudinal stiffeners with the proposed geometrical properties welded to the web of a composite beam eliminate local buckling and enhance its rotation capacity in hogging moment regions.
- A simplified model based on a linear moment–axial compression relationship is proposed for use in the design of composite beams.

As a further conclusion, it needs to be emphasized that for design purposes an approach that gives an intermediate interaction strength somewhere between the RPA envelope and the FEM analysis envelope (with reference to Fig. 8) would seem to be a more accurate design approach. This method should rely on RPA but should also consider the calculation of the beam deflections at failure by a plastic analysis approach in order to account for the secondary moments. This is a separate field of research to be considered in the future for providing the designers a robust design approach for new composite beams as well as for the assessment of the over-strength of existing infrastructure.

Acknowledgements

The experimental research presented in this paper was funded by the Australian Research Council (ARC) Discovery Project DP0879734. The authors would also like to thank Dr Mithra Fernando and all the technical staff of the Structures Laboratory at the University of Western Sydney for their valuable assistance with the experimental work.

References

[1] Banfi M. Composite beams with web openings subject to axial load. EUROSTEEL 2008; September 3–5 2008. Graz, Austria.
[2] Eurocode 4. Design of composite steel and concrete structures. London (UK): British Standards Institution; 2004.
[3] Standards Australia. Composite structures part 1: simply supported beams. AS 2327.1-2004. Sydney (Australia); 2004.
[4] ANSI/AISC 360-05. Specification for structural steel buildings. Chicago (IL, USA): American Institute of Steel Construction; 2005.
[5] Chapman JC, Balakrishnan S. Experiments on composite beams. Struct Eng 1964;42(11):369-83.
[6] Ansourian P. Experiments on continuous composite beams. Proc Inst Civ Eng Part 2 1982;73(1):26-51.
[7] Nie J, Fan J, Cai CS. Experimental study of partially shear connected composite beams with profiled sheeting. Eng Struct 2008;30(1):1–12.
[8] Vasdravellis G, Uy B, Tan EL, Kirkland B. The effects of axial tension on the hogging-moment regions of composite beams. J Constr Steel Res 2012;68(1):20-33.
[9] Vasdravellis G, Uy B, Tan EL, Kirkland B. The effects of axial tension on the sagging-moment regions of composite beams. J Constr Steel Res 2012;72:240-53.
[10] Uy B, Bradford MA. Cross-sectional deformation of prestressed composite tee-beams. Struct Eng Rev 1993;5(1):63-70.
[11] Uy B. Long term behaviour of composite steel–concrete beams prestressed with high strength steel tendons. Advances in Steel Structures (ICASS '96); 1996. p. 419-24.
[12] Nie J, Tang L, Cai CS. Performance of steel–concrete composite beams under combined bending and torsion. J Struct Eng 2009;135(9):1048-57.
[13] Tan EL, Uy B. Experimental study on straight composite beams subjected to combined flexure and torsion. J Constr Steel Res 2009;65(4):784-93.

[14] Tan EL, Uy B. Experimental study on curved composite beams subjected to combined flexure and torsion. J Constr Steel Res 2009;65(8–9):1855-63.
[15] Baskar K, Shanmugam NE. Steel–concrete composite plate girders subject to combined shear and bending. J Constr Steel Res 2003;59(4):531-57.
[16] Elghazouli AY, Treadway J. Inelastic behaviour of composite members under combined bending and axial loading. J Constr Steel Res 2008;64(9):1008-19.
[17] Uy B, Tuem HS. Behaviour and design of composite steel–concrete beams under combined actions 2006. Eighth international conference on steel–concrete composite and hybrid structures (ICSCCS 2006), Harbin, China; 2006. p. 286-91.
[18] Deric JO, Bradford MA. Elementary behaviour of composite steel and concrete structural members. Oxford: Butterworth-Heinemann; 1999.
[19] ABAQUS user's manual, version 6.9. Pawtucket, RI: Hibbit, Karlsson & Sorenson; 2005.
[20] Carreira DJ, Chu KH. Stress–strain relationship for plain concrete in compression. ACI J 1985;82(11):797-804.
[21] Eurocode 3. Design of steel structures. London (UK): British Standards Institution; 2005.
[22] Johnson RP. Composite structures of steel and concrete. Volume 1: Beams, slabs, columns, and frames for buildings. Oxford: Blackwell Scientific Publications; 1994.
[23] Trahair NS, Bradford MA, Nethercot DA. The behaviour and design of steel structures to BS5950. London: Spon Press; 2001. Third edition — British.
[24] Bruneau M, Uang CM, Whittaker A. Ductile design of steel structures. USA: McGraw-Hill; 1998.
[25] Standards Australia. Steel structures. AS4100. Sydney (Australia); 1998.